Kim, K.-C., Shprits, Y. (2018): Survey of the Favorable Conditions for Magnetosonic Wave Excitation. - *Journal of Geophysical Research*, *123*, 1, pp. 400—413.

DOI: http://doi.org/10.1002/2017JA024865

AGU PUBLICATIONS

JGR

Journal of Geophysical Research: Space Physics

RESEARCH ARTICLE

10.1002/2017JA024865

Survey of the Favorable Conditions for Magnetosonic Wave Excitation

Kyung-Chan Kim[1] and **Yuri Shprits**[2,3,4]

[1]Division of Science Education, College of Education, Daegu University, Gyeongsan, Gyeongbuk, South Korea, [2]Helmholtz Centre Potsdam, GFZ German Research Centre for Geosciences, Potsdam, Germany, [3]Institute of Physics and Astronomy, University of Potsdam, Potsdam, Germany, [4]Department of Earth, Planetary, and Space Sciences, University of California, Los Angeles, CA, USA

Key Points:
- There is a statistically significant relationship between occurrences of proton rings and magnetosonic waves
- We statistically examine how the ratio of the ring energy to the Alfven energy affect magnetosonic wave excitation
- Different values of the ratio for exciting magnetosonic waves outside and inside the plasmapause are found

Correspondence to:
K.-C. Kim,
kyungchan80@gmail.com

Citation:
Kim, K.-C., & Shprits, Y. (2018). Survey of the favorable conditions for magnetosonic wave excitation. *Journal of Geophysical Research: Space Physics*, *123*, 400–413. https://doi.org/10.1002/2017JA024865

Received 8 OCT 2017
Accepted 28 DEC 2017
Accepted article online 3 JAN 2018
Published online 17 JAN 2018

Abstract The ratio of the proton ring velocity (V_R) to the local Alfven speed (V_A), in addition to proton ring distributions, plays a key factor in the excitation of magnetosonic waves at frequencies between the proton cyclotron frequency f_{cp} and the lower hybrid resonance frequency f_{LHR} in the Earth's magnetosphere. Here we investigate whether there is a statistically significant relationship between occurrences of proton rings and magnetosonic waves both outside and inside the plasmapause using particle and wave data from Van Allen Probe-A during the time period of October 2012 to December 2015. We also perform a statistical survey of the ratio of the ring energy (E_R, corresponding to V_R) to the Alfven energy (E_A, corresponding to V_A) to determine the favorable conditions under which magnetosonic waves in each of two frequency bands ($f_{cp} < f \leq 0.5\ f_{LHR}$ and $0.5\ f_{LHR} < f < f_{LHR}$) can be excited. The results show that the magnetosonic waves in both frequency bands occur around the postnoon (12–18 magnetic local time, MLT) sector outside the plasmapause when E_R is comparable to or lower than E_A, and those in lower-frequency bands ($f_{cp} < f \leq 0.5\ f_{LHR}$) occur around the postnoon sector inside the plasmapause when $E_R/E_A > \sim 9$. However, there is one discrepancy between occurrences of proton rings and magnetosonic waves in low-frequency bands around the prenoon sector (6–12 MLT) outside the plasmapause, which suggests either that the waves may have propagated during active time from the postnoon sector after being excited during quiet time, or they may have locally excited in the prenoon sector during active time.

1. Introduction

Fast magnetosonic waves (first called equatorial noise by Russell et al., 1970) are whistler-mode electromagnetic emissions observed in the Earth's magnetosphere occurring in the frequency range between the proton cyclotron frequency (f_{cp}) and the lower hybrid resonance frequency (f_{LHR}). These waves are also named as ion Bernstein waves, which are perhaps more appropriate term in theoretical point of view not to be confused with the traditional "magnetosonic" mode that exists much below f_{cp} in magnetohydrodynamics theory (Gary et al., 2010). In this manuscript we will simply use phenomenologically described term "magnetosonic wave" common in recent literature. They are usually observed within a few degrees of the magnetic equator both outside and inside the plasmasphere and propagate at sufficiently large angles to the ambient magnetic field (Hrbáčková et al., 2015; Kasahara et al., 1994; Kim & Chen, 2016; Laakso et al., 1990; Ma et al., 2013; Meredith et al., 2008; Russell et al., 1970; Santolík et al., 2002). Recently, much attention has been paid to the properties and spatial distribution of the magnetosonic waves and their possible role in the radiation belt dynamics contributing to both acceleration and loss of relativistic electrons (e.g., Horne et al., 2007; Shprits, 2016; Shprits et al., 2013). It is generally accepted that a ring distribution of protons with positive gradient in the phase space density provides a source of free energy for the excitation of magnetosonic waves, which forms at energies of the order of 10 keV (Balikhin et al., 2015; Boardsen et al., 1992; Chen et al., 2010, 2011; Curtis & Wu, 1979; Horne et al., 2000; Ma et al., 2014; Perraut et al., 1982). Theoretical analysis and simulations have verified excitation of fast magnetosonic waves (Convery & Gary, 1997; Gary et al., 2010; Liu et al., 2011; Min et al., 2017; Umeda et al., 2007, 2012).

The ratio of the ring energy (E_R), corresponding to the peak in the phase space density (PSD), to the Alfven energy (E_A), corresponding the local Alfven speed that is related to the total plasma density and the background magnetic field intensity, is a key factor controlling the excitation of magnetosonic waves. Horne et al. (2000) suggested that wave growth is possible when the ring velocity (V_R) exceeds the Alfven speed (V_A) within a factor of 2. Meredith et al. (2008) made the first observational attempt, using particle and

wave data from the Combined Release and Radiation Effects Satellite (CRRES), to understand a link between proton ring distributions and magnetosonic waves in the frequency band 0.5 $f_{LHR} < f < f_{LHR}$ during geomagnetically active conditions. They found the close coincidence between the magnetic local time (MLT) distributions of the observed wave amplitude and proton ring distributions satisfying $E_R > E_A$. However, they also found the enhanced waves in the dawn sector outside the plasmapause that do not satisfy $E_R > E_A$. More recently, Chen et al. (2010) presented, based on ring current ion simulation during the storm main phase incorporating the Rice Convection Model into Ring Current-Atmospheric Interactions Model, the excited frequency dependence according to the ratio E_R/E_A and suggested that the unstable frequency band of waves inside the plasmapause becomes lower than outside due to an increase in plasma density, leading to an increase in the ratio E_R/E_A. Ma et al. (2014) also presented the different values of E_R/E_A for exciting magnetosonic waves in three different regions, outside, near, and deep inside the plasmapause, based on a case study comparing the Time History of Events and Macroscale Interactions during Substorms observations and wave growth rate estimated using plasma instability analysis.

The goal of this study is to present a comparison of global distributions of proton rings and magnetosonic waves and to determine critical values of the ratio E_R/E_A under which magnetosonic waves are likely to be excited. For this study, we perform a statistical survey of the occurrences of proton ring distributions and magnetosonic waves both outside and inside the plasmapause using particle and wave data from Van Allen Probe-A during the time period of October 2012 to December 2015, which is in line with the previous study of Meredith et al. (2008), but we extend the analysis to lower-frequency bands ($f_{cp} < f \leq 0.5\ f_{LHR}$) with the extensive coverage over all MLT sectors from Van Allen Probe-A while they only focused on upper-frequency bands ($0.5\ f_{LHR} < f < f_{LHR}$) with the lack of wave coverage on the dawn sector using CRRES. Previous studies (Chen et al., 2010, 2011; Ma et al., 2014) suggested, based only on specific events, that wave growth is possible even if E_R is slightly lower than or comparable to E_A. However, there has been no statistical analysis that examines how the ratio E_R/E_A affect magnetosonic wave excitation. Thus, in this study, we perform a statistical survey of the ratio E_R/E_A and compare it with the distribution of magnetosonic waves separately in two frequency bands, the low ($f_{cp} < f \leq 0.5 f_{LHR}$) and high ($0.5 f_{LHR} < f < f_{LHR}$) bands.

The remainder of this paper is organized as follows. The global distributions of energetic protons in terms of flux and PSD both outside and inside the plasmapause under various levels of magnetic activity are presented in section 2, the relation between occurrences of magnetosonic waves and proton rings is presented in section 3, the global distributions of the ratio E_R/E_A and magnetosonic waves separately in two frequency bands are presented in section 4, and the discussion and conclusions are given in sections 5 and 6, respectively.

2. Spatial Distribution of Energetic Protons

The twin Van Allen Probes have operated in a highly elliptical geosynchronous transfer orbit since their launch on 30 August 2012, with an apogee of ~5.8 R_E, a perigee of ~700 km, an inclination of ~10°, and a period of ~9 h (Mauk et al., 2012). For this study, we use proton fluxes from the Helium Oxygen Proton Electron (HOPE) plasma spectrometer, a part of the Energetic particle, Composition, and Thermal plasma (ECT) suite (Funsten et al., 2013) on board the Van Allen Probes. The ECT/HOPE provides the proton differential fluxes in the pitch angle range from 0° to 180° with a resolution of ~15° in the energy ranges 1 eV $< E <$ 50 keV with 36 logarithmic spaced energy channels.

To understand how energetic particles injected during substorms form an unstable proton ring distribution, we first show in Figure 1 the global distribution of the proton differential flux for a pitch angle of 90°, $j_\perp$, outside the plasmapause during three levels of geomagnetic activity, measured by *AE** (the maximum value of the *AE* index in the previous 3 h) for protons of energy between 527 eV and 20686 eV. Here the average value of the data collected as a function of L^* in steps of 0.2 L^* for $2 \leq L^* \leq 6$ and MLT with 1 h intervals during the time period of October 2012 to December 2015 from Van Allen Probe-A ECT/HOPE is displayed using a logarithmic scale regardless of whether the magnetosonic waves occur. The L^* parameter used in this study is related to the third adiabatic invariant and has physical meaning of the radial distance from the center of the Earth to the equatorial crossing points of a drift shell on which particles drift about the Earth if the magnetic field is adiabatically changed to a dipole (Roederer, 1970). Database for the L^* and MLT is taken from Van Allen Probes-ECT data portal (https://rbsp-ect.lanl.gov/data_pub/rbspa), and we simply assumed

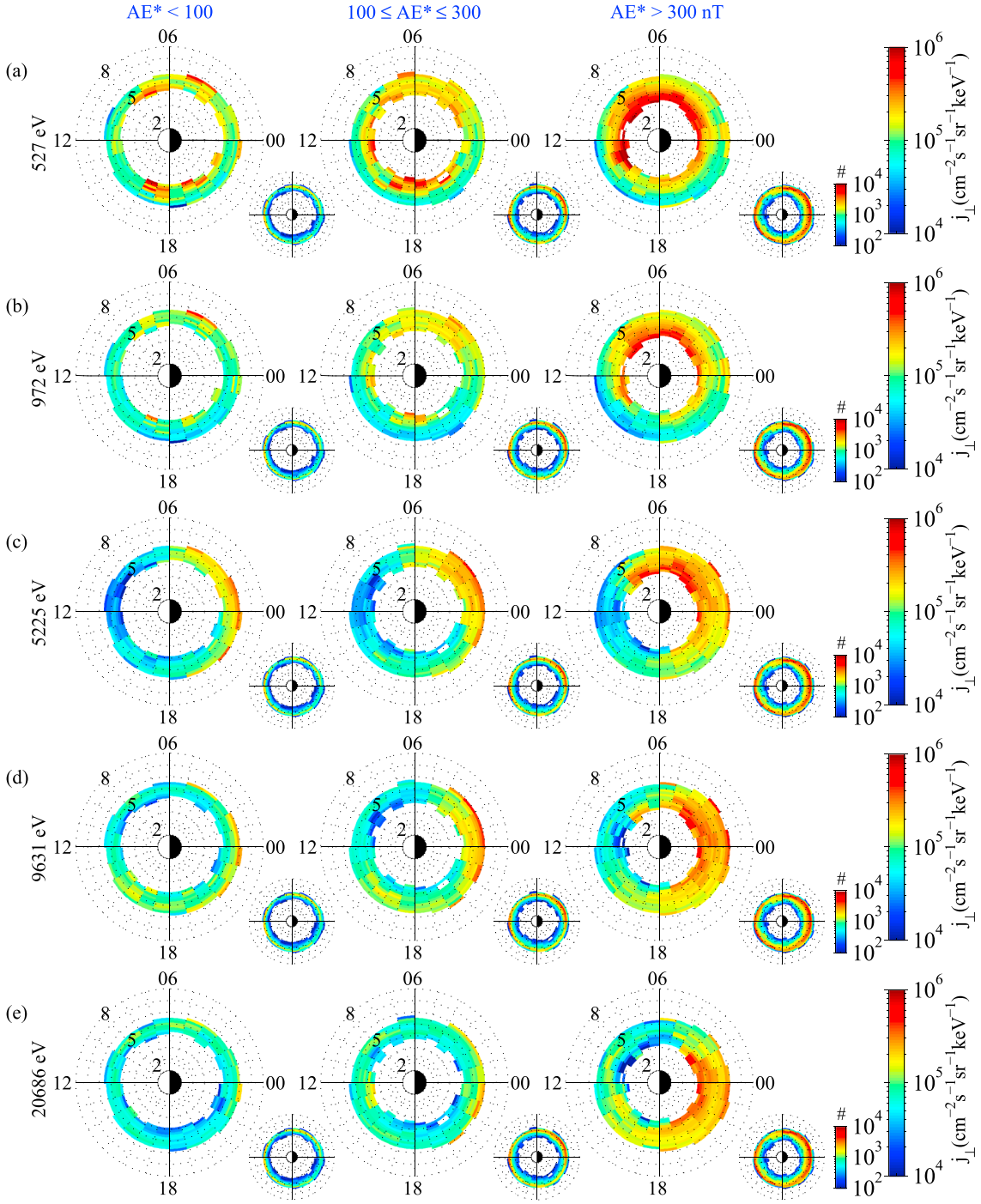

Figure 1. Global average proton flux maps for five energy channels outside the plasmapause during different activity levels of *AE**. The number of samples in each panel is displayed in the small panel. Only the bins with the number of data of >100 were displayed.

locally mirroring particles at the satellite location in the use of L^* using the TS04D (Tsyganenko & Sitnov, 2005) magnetic field model. Only the measurements made within 10° of the magnetic equator were considered, and data in the region $L^* \leq 2$ were removed due to the possibility of contamination for the proton radiation belt. The plasmapause location is identified using wave spectra from a single electric component of waves between 10 kHz and 400 kHz from the High-Frequency Receiver (HFR), a part of the Electric and Magnetic Field Instrument Suite and Integrated Science (EMFISIS) instrumentation suite (Kletzing et al.,

2013), when a sudden change in intensity of the electrostatic electron-cyclotron harmonic (ECH) waves, integrated over the frequency range between 2.5 f_{ce} (f_{ce} is the electron gyrofrequency) and 5.0 f_{ce}, is detected per half orbit, since high intensity of the ECH is usually observed outside the plasmapause (Meredith et al., 2004). In addition, the appearance and disappearance of the whistler mode chorus between $0.1f_{ce}$ and $0.8f_{ce}$ and plasmaspheric hiss between 40 Hz and 2 kHz from the Waveform Receiver (WFR), another part of EMFISIS, and a sharp gradient in plasma density, inferred from EMFISIS, are used to manually modify the plasmapause's location determined above. An example will be given in Figure 4.

The nightside proton flux for all energies increases with increasing *AE** by roughly half an order of magnitude for each level. During active conditions, particles can penetrate as low as $L^* = 3$, and the flux peak tends to shift from the prenoon sector toward the midnight sector with increasing energy, due to the energy-dependent drift, that is, westward gradient-curvature drift that is dominant for >10 keV and eastward electric field drift that is dominant for several keV (Korth et al., 1999; Lyons & Williams, 1984). With the accompanying shift in peak of flux, the region where proton flux for ≥972 keV remains low shifts from the postnoon toward the prenoon sector with increasing energy regardless of geomagnetic activity (though it is clearly seen for active conditions), possibly either due to lack of protons that access that region after substorm injection or loss of protons by charge exchange and/or Coulomb collisions (Fok et al., 1995, 1996; Jordanova et al., 1996, 1999).

The global distribution of proton energy fluxes inside the plasmapause is shown in Figure 2, in the same format as Figure 1. Proton fluxes inside the plasmapause are generally lower than those outside the plasmapause (note the different color scales in Figures 1 and 2) but with no discernable dependence on *AE**. An interesting feature is that, as shown in Figure 1, the MLT region of the flux dip tends to be around the postnoon sector for low-energy protons (≤ 972 eV) and around the prenoon sector for high-energy protons (> 972 eV).

To examine how such variations in flux are seen in variations in PSD, we converted the proton differential flux at each measurement into PSD using

$$f_{\perp} = 0.5449 \cdot \frac{j_{\perp}}{E} \tag{1}$$

where $f_{\perp}$ is the PSD given in $m^{-6}\ s^3$, $j_{\perp}$ is the proton differential flux with 90° pitch angle in units of $cm^{-2}\ s^{-1}\ sr^{-1}\ keV^{-1}$, E is the effective energy of the proton energy channel in keV, and 0.5449 is a conversion factor from $j_{\perp}$ to $f_{\perp}$ for protons (Lyons & Williams, 1984).

The average PSD $f_{\perp}$ variation as a function of energies up to ~50 keV for four MLT sectors (0–6 MLT, 6–12 MLT, 12–18 MLT, and 18–24 MLT) and three *AE** activities ($AE^* < 100$ for quiet, $100 \le AE^* \le 300$ for moderate, and $AE^* > 300$ nT for active) is presented in Figures 3a and 3b, each for outside and inside the plasmapause. Here the PSD $f_{\perp}$ at a given energy is estimated by first sorting and averaging the converted PSD $f_{\perp}$ using equation (1) at each measurement in each 0.2 L^* and 1 MLT bin and then averaging all PSDs across all L^* in each MLT sector at a given energy.

A proton ring distribution is present around the postnoon sector ($12 \le \text{MLT} < 18$, third columns) on both sides of the plasmapause, having the peak energy of the proton ring at ~10 keV outside the plasmapause and at slightly lower energy inside the plasmapause, with a weak dependence on *AE** (though it becomes clearer for low activity). It is also found in the prenoon sector ($6 \le \text{MLT} < 12$) outside the plasmapause with a peak energy of ~10 keV during quiet time. Note that the less pronounced ring distributions are due to averaging that might reduce the peak in phase space density. Consequently, we can see from Figures 1–3 that variations in flux around the prenoon and postnoon sectors driven by the energy-dependent drift and loss lead to proton ring distributions in PSD at the energies of ~10 keV, consistent with previous studies (e.g., Boardsen et al., 1992, Horne et al., 2000, Thomsen et al., 2011).

3. Spatial Distribution of Proton Rings and Magnetosonic Waves

Proton rings with positive gradient in the perpendicular velocity distribution to the magnetic field provide a source of free energy that can excite magnetosonic waves. Here we present the global distributions of the proton rings in velocity space and the magnetosonic waves for both sides of the plasmapause to examine the relationship between them.

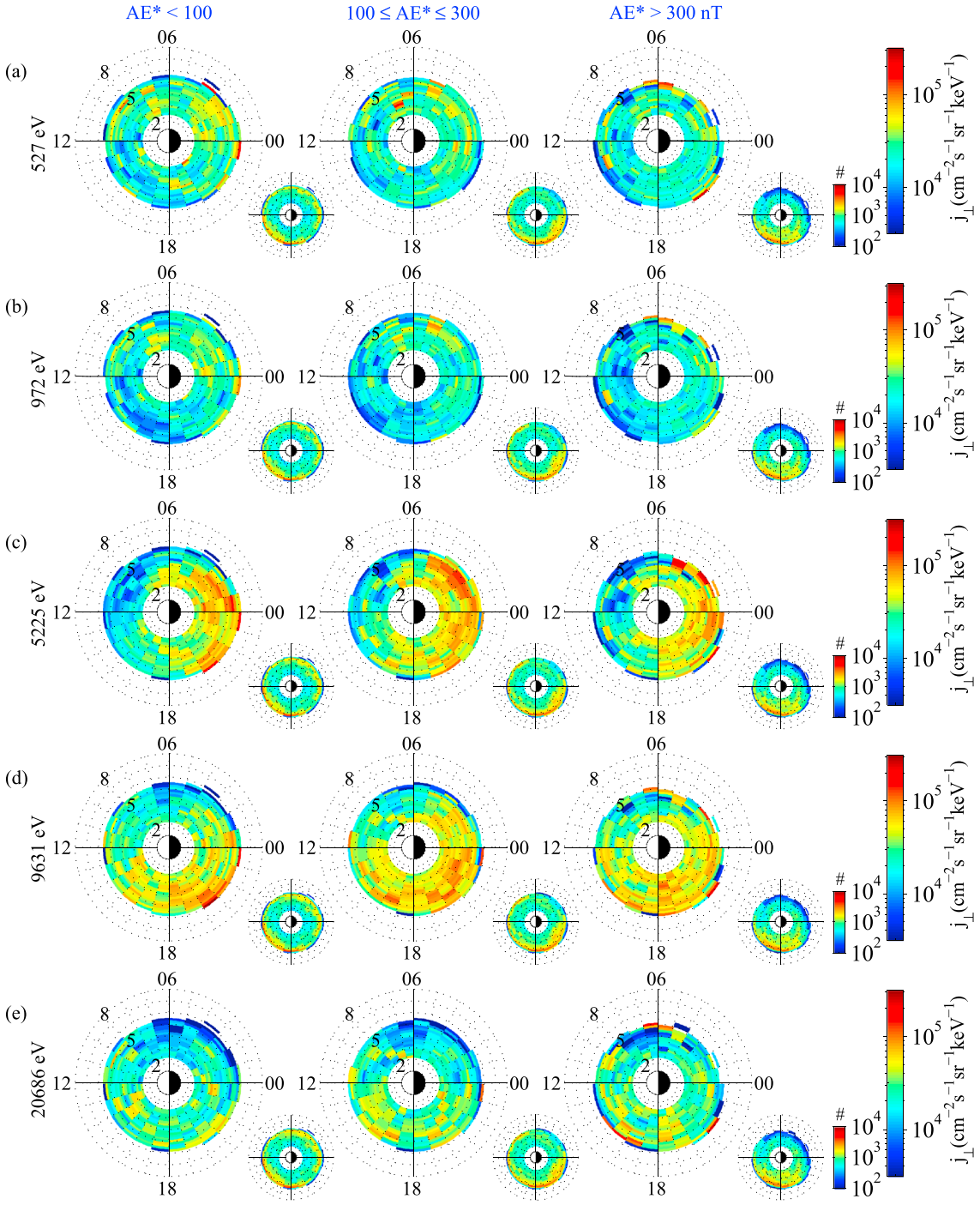

Figure 2. The same as in Figure 1 but for the case inside the plasmapause.

We first introduce the methodology that identifies the proton rings and the magnetosonic wave signals from Van Allen Probe-A. Proton ring distributions from the perpendicular PSD as a function of energy, $f_{\perp}(E)$, smoothed using a moving average filter for every measurement, are identified using the following conditions: (1) the value of $f_{\perp}$ increases continuously over at least three consecutive energy channels; (2) the $f_{\perp}$ of the peak is larger than 10^{-15} m^{-6} s^{3} (which is comparable to that of Horne et al., 2000); and (3) a clear dip of $f_{\perp}$, whose $f_{\perp}$ value is smaller than all other $f_{\perp}$ values at energies close to the peak energy, exists. The

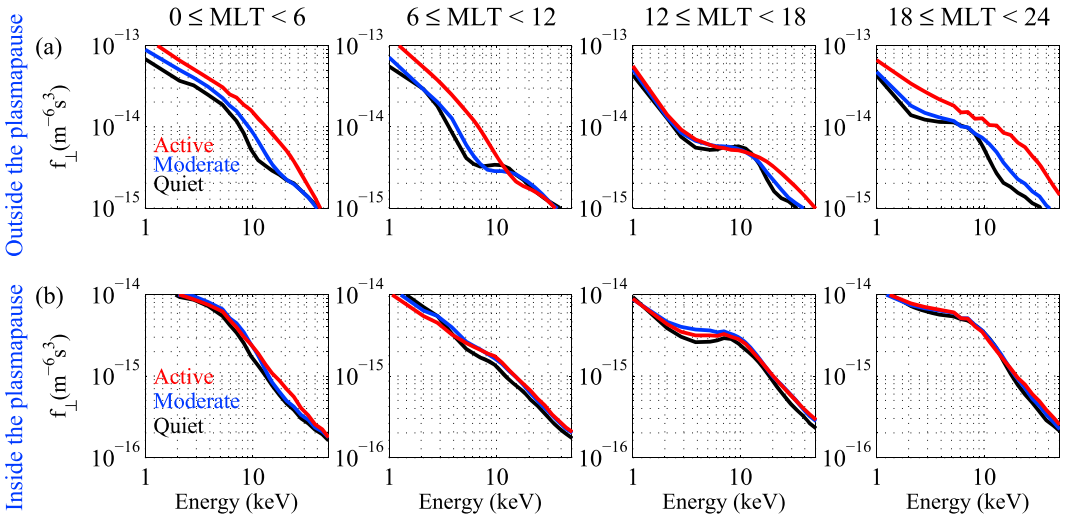

Figure 3. The average PSD $f_\perp$ variation for four MLT sectors during three levels of *AE** (a) outside and (b) inside the plasmapause.

criteria can be satisfied at multiple peak energies in the energy range of interest (1–50 keV). In such cases, we identify the peak with the lowest energy as the proton ring. Highly oblique magnetosonic waves are captured from wave spectra covering the frequency range from 10 Hz up to 12 kHz for all three components of both magnetic and electric fields from EMFISIS/WFR when the criteria of wave normal angle of ≥80° and the absolute value of wave ellipticity of ≤0.2 both sides of the plasmapause (Li et al., 2015; Ma et al., 2016; Němec et al., 2013) using the singular value decomposition method (Santolík et al., 2003) are satisfied. In this study, we simply identified highly oblique magnetosonic waves in a conventional way assuming emissions that typically have large wave normal angles close to ~90° and low ellipticity close to 0 (and thus nearly linearly polarized). Note that our database of wave emission might also contain other types of waves, mostly kinetic Alfven waves that are right-hand polarized and magnetically compressive waves like magnetosonic waves (e.g., Moya et al., 2015; Salem et al., 2012) or they might miss zipper-like magnetosonic waves that have ellipticity higher than 0 (e.g., Li et al., 2017).

An example of the variation in PSD $f_\perp$ observed by Van Allen Probe-A on 13 November 2012 is present in Figure 4a, overlaid with ring energy (black dot), dip energy (white dot), and Alfven energy (blue line). Here the Alfven energy (E_A) is estimated using

$$E_A = \frac{1}{2} m_p V_A^2 \tag{2}$$

where the Alfven speed (V_A) is obtained by assuming single-ion (H^+) plasma and given by

$$V_A = \frac{B}{\sqrt{\mu_0 m_p N}} \tag{3}$$

where μ_0 is the vacuum permeability, m_p is the proton mass, N is the plasma number density, inferred from EMFISIS by applying the Neural-network-based Upper hybrid Resonance Determination algorithm (Zhelavskaya et al., 2016), and B is the background magnetic field intensity, taken from measurements from EMFISIS. Figures 4b–4g show wave spectra of electric field from HFR overlaid with harmonics of f_{ce} up to 5.0 f_{ce} (Figure 4b), wave spectra of magnetic and electric field from WFR (Figures 4c and 4d), wave normal angle (Figure 4e), signed ellipticity (Figure 4f), and wave flag (Figure 4g). In Figures 4c–4f, curves for f_{ce}, $0.5f_{ce}$, $0.1f_{ce}$, f_{LHR}, $0.5f_{LHR}$, and f_{cp}, from top to bottom, are overlaid. The value of f_{LHR} is estimated as $\sqrt{f_{cp} f_{ce}}$. In Figure 4g, the identified magnetosonic wave signals are indicated by black and red for regions outside and inside the plasmapause, respectively. The vertical black and blue lines indicate, respectively, the plasmapause location and the perigee time of each orbit.

Based on the criteria above, we identified the proton rings and magnetosonic wave amplitudes, the root-mean square by integrating over the frequency range between f_{cp} and f_{LHR}, during the time period of

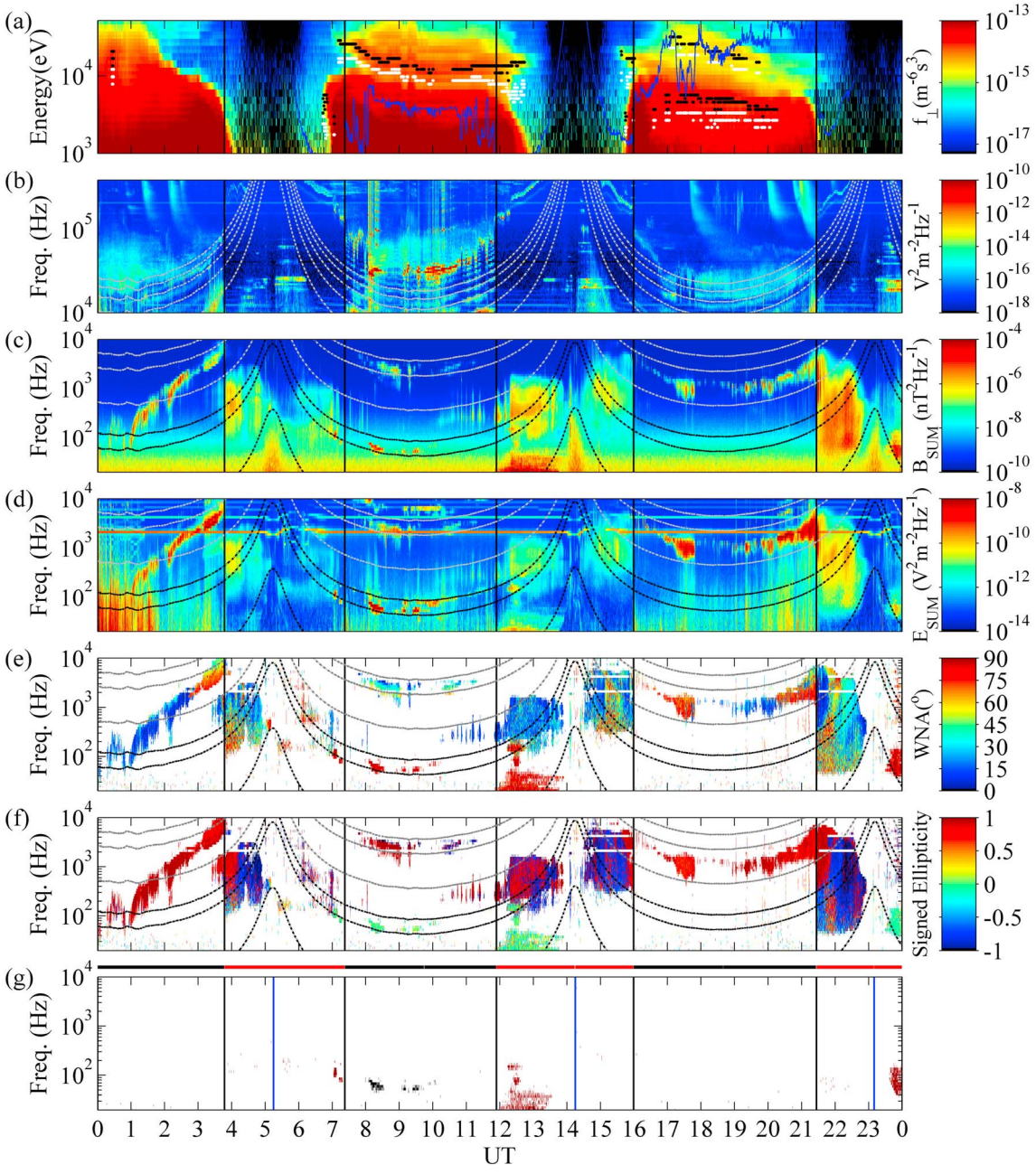

Figure 4. An example of the variation in PSD $f_\perp$ and magnetosonic wave signals observed by Van Allen Probe-A on 13 November 2012. (a) Proton PSD perpendicular to the magnetic field as a function of energy measured by HOPE, (b) wave electric intensity spectrograms measured by HFR, (c and d) magnetic and electric wave spectra measured by WFR, (e) wave normal angle (deg), (f) signed ellipticity, and (g) wave flag. The vertical black and blue lines are the plasmapause location and the perigee time of each orbit, respectively. Also shown in Figure 4a is ring energy (black dot), dip energy (white dot), and Alfven energy (blue line). Harmonics of f_{ce} up to 5.0 f_{ce} in Figure 4b, and f_{ce}, $0.5f_{ce}$, $0.1f_{ce}$, f_{LHR}, $0.5f_{LHR}$, and f_{cp}, from top to bottom, in Figures 4c–4f are denoted as curves.

October 2012 to December 2015. Note that the magnetosonic wave amplitudes in the lower-frequency band ($f_{cp} < f \leq 0.5\ f_{LHR}$) may be underestimated at $L^* \geq 3.6$, since the lowest frequency covered by Van Allen Probes EMFISIS/WFR is 10 Hz. Nevertheless, the occurrence rate and amplitudes of the lower-frequency band are considerably higher than those of the higher-frequency band (which will be presented below), and thus it is sufficient to investigate the relationship between the occurrences of proton rings and lower-frequency band.

Figure 5 shows the spatial distribution of (a, b, e and f) proton rings and (c, d, g, and h) magnetosonic wave amplitude over the frequency range between f_{cp} and f_{LHR} with their occurrence rate both (a–d) outside and

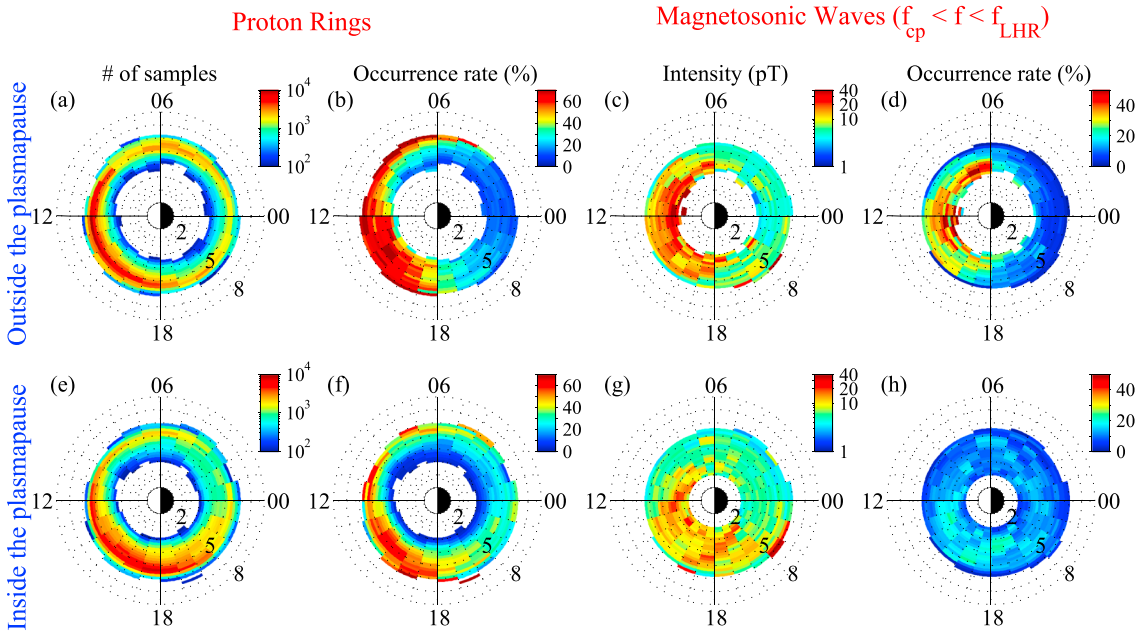

Figure 5. Global distributions of (a and e) the number of proton rings and (b and f) the corresponding occurrence rate (%) and (c and g) the average magnetosonic wave amplitude, and (d and h) the corresponding occurrence rate (%) outside (Figures 5a–5d) and inside (Figures 5e–5h) the plasmapause.

(e–h) inside the plasmapause. The occurrence rate is defined in percentage as proton ring (or wave) measurement time divided by the dwelling time of spacecraft in each bin of L^* and MLT. The same database of magnetosonic wave signals were taken from Kim and Shprits (2017) where it was binned in terms of McIlwain L value (McIlwain, 1961), but we binned it as a function of L^*. The only difference between their and ours is that waves at high L value maps to a relatively low L^* (comparison is between Figure 2 of Kim & Shprits, 2017 and Figure 5).

High occurrence ($\geq$ ~50%) of proton rings (Figures 5b and 5f) is observed from both outside and inside the plasmapause in the postnoon sector (12–18 MLT) over a broad range of L^*, through outside the plasmapause in the noon sector, to outside the plasmapause in the prenoon sector (6–12 MLT) at $L^* \geq 5$. This is generally consistent with regions of relatively high occurrence of magnetosonic waves (Figures 5d and 5h) on the dayside on both sides of the plasmapause, except for outside the plasmapause in the prenoon sector at $L^* \leq 5$, where an opposite tendency is observed: relatively low occurrence ($<$ 20%) in the proton rings against other regions and higher occurrence in the magnetosonic waves. The discrepancy between the occurrences of proton rings and magnetosonic waves is also found in the previous study of Meredith et al. (2008) where they presented intense waves of high-frequency band ($0.5f_{LHR} < f < f_{LHR}$) in the dawn sector, which do not show the ring distribution.

For a clearer examination of the relationship between proton rings and magnetosonic waves, the rate of existence of proton ring distributions during the time when magnetosonic waves occur regardless of its intensity is also presented in Figures 6a and 6b, each for outside and inside the plasmapause. More than 60% of all wave measurement time is observed simultaneously with the proton ring distributions in the postnoon sector on both sides of the plasmapause, implying that proton rings are a potential source of the magnetosonic waves, while only less than 10% of them are observed with proton ring distributions in the prenoon sector outside the plasmapause.

4. Relationship Between the Ratio E_R/E_A and the Excitation of Magnetosonic Waves in Two Frequency Bands

Above, we have found that proton ring distributions closely match the distribution of magnetosonic waves except for that in the prenoon sector outside the plasmapause, which implies that the existence of proton ring distribution is a necessary condition for the excitation of magnetosonic waves. It is known that Alfven

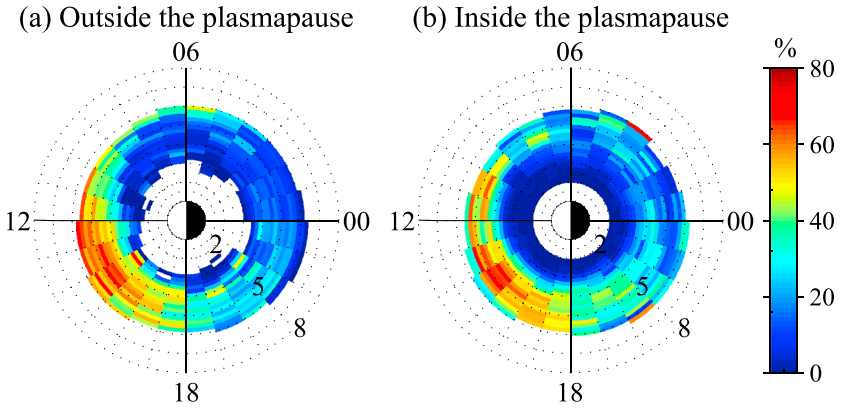

Figure 6. The occurrence rate of proton ring distributions simultaneously during the time when magnetosonic waves occur (a) outside and (b) inside the plasmapause.

energy E_A is a key factor in controlling the magnetosonic wave growth by changing the ratio E_R/E_A. In this section, we investigate how variations in E_A affect the magnetosonic wave excitation and determine statistically critical ratio E_R/E_A exciting (or inhibiting) magnetosonic waves, separately, for two frequency bands both outside and inside the plasmapause. For this analysis, we separated the magnetosonic waves over the whole frequency range shown in Figure 5 into two frequency bands: low ($f_{cp} < f \leq 0.5f_{LHR}$) and high ($0.5f_{LHR} < f < f_{LHR}$) bands.

The global distribution of median proton ring energy E_R outside the plasmapause is shown in Figure 7a, and the corresponding ratio E_R/E_A in Figure 7b, together with the median absolute deviation in the small panels. The global distribution of the average wave intensity for lower- and higher-frequency bands is also

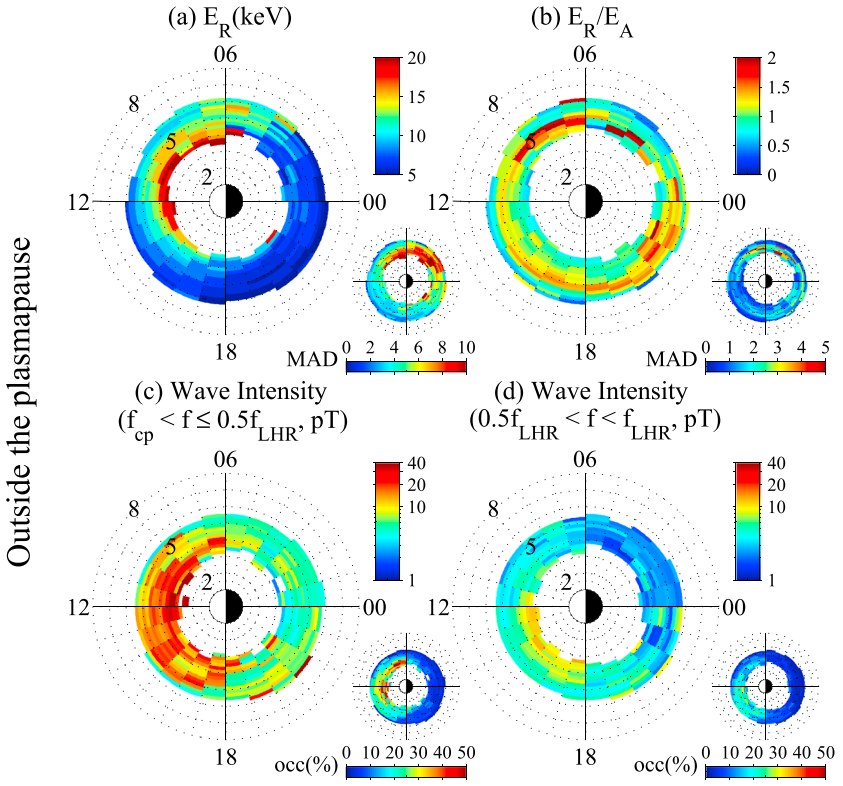

Figure 7. Comparison of (a) E_R and (b) E_R/E_A and (c and d) magnetosonic wave intensity for two frequency bands outside the plasmapause. Also shown in the small panels are the median absolute deviation in Figures 7a and 7b and the occurrence rates in Figures 7c and 7d.

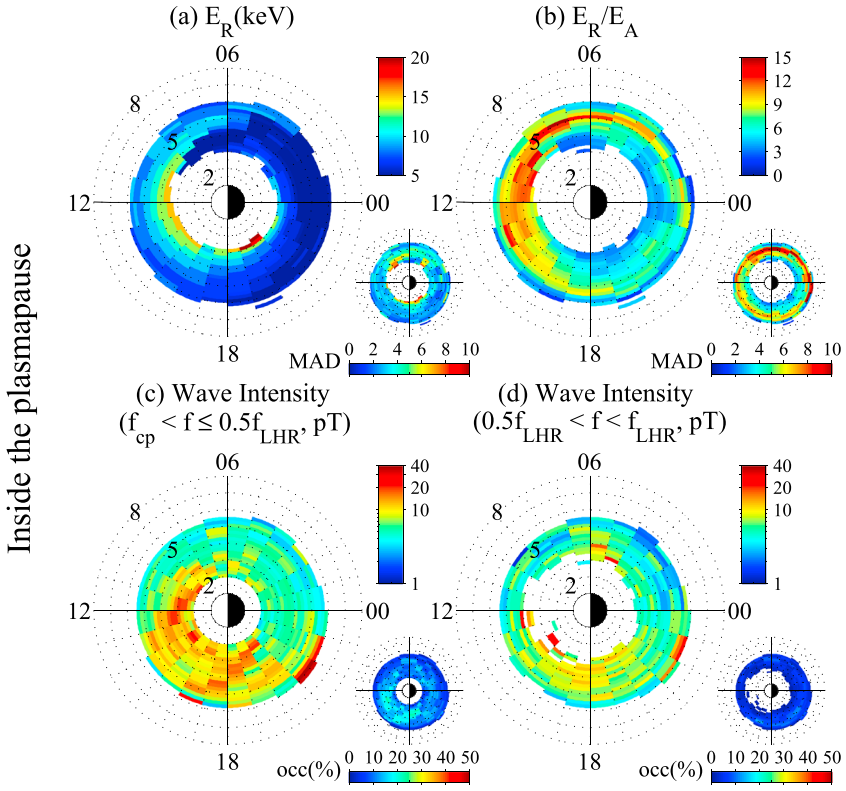

Figure 8. Same as in Figure 7 but for the case inside the plasmapause.

presented in Figures 7c and 7d, respectively, together with the corresponding occurrence rates in the small panels. One can see by comparing Figure 7c with Figure 5c that occurrences of magnetosonic waves outside the plasmapause shown in Figure 5c are mostly attributed to those of lower-frequency bands. The ring energy ranges from a few to a few tens of keV with the highest values in the 6–14 MLT sector. A relatively low ratio E_R/E_A ($\leq$~1) with low spreads is present in the region from 21 MLT at $L^* \leq 5$, through the noon sector at $L^* \leq 5$, to 9 MLT at $L^* \leq 4.5$. In general, the distribution is consistent with that of magnetosonic waves in both bands, having more similarity with higher-frequency bands, although it is difficult to make a direct comparison between occurrences of magnetosonic waves and the ratio E_R/E_A in the prenoon sector at $L^* \leq 4$ due to lack of data for E_R/E_A. The result is similar to the previous studies (Chen et al., 2010; Ma et al., 2014) where they suggested that proton rings with E_R just below E_A provide a free energy to excite the magnetosonic waves, especially in high-frequency bands, outside the plasmapause.

Figure 8 shows the results for the case inside the plasmapause. Peak of ring energy shifts more toward the noon sector than outside. The ratio E_R/E_A (Figure 8b) is generally higher than outside the plasmapause shown in Figure 7b (note the different color scales in Figures 7b and 8b) due to a decrease in E_A in the high-plasma density region, while the remaining E_R is similar to that outside the plasmapause. The ratio E_R/E_A less than ~9 (with deviation of ~3) is present over a broad MLT range from 14, through midnight, to 9 at $L^* <$ ~5 where magnetosonic waves in lower-frequency bands mostly occur inside the plasmapause with a peak occurrence rate near the postnoon sector, while there exist very rare magnetosonic waves in the region where $E_R/E_A >$ ~9, mostly near the prenoon sector at high $L^* > 3.5$, which seems to inhibit exciting magnetosonic waves. Also, the distribution of intense high-frequency bands around the dusk sector well matches that of $E_R/E_A <$ ~9, but its occurrence is very low (< 5%). Note that the value of 9 corresponds to 3 when the ratio of the proton ring velocity to the Alfven speed V_R/V_A is estimated, which is suggested by Chen et al. (2010) as the upper limit of exciting the lower magnetosonic wave band inside the plasmapause. We thus have confirmed that, as suggested by Chen et al. (2010), as plasma density increases, that is, inside the plasmasphere, V_R/V_A (thus E_R/E_A) increases (due to the inverse relation between V_A and the plasma density), and the unstable frequency band shifts toward the lower frequencies.

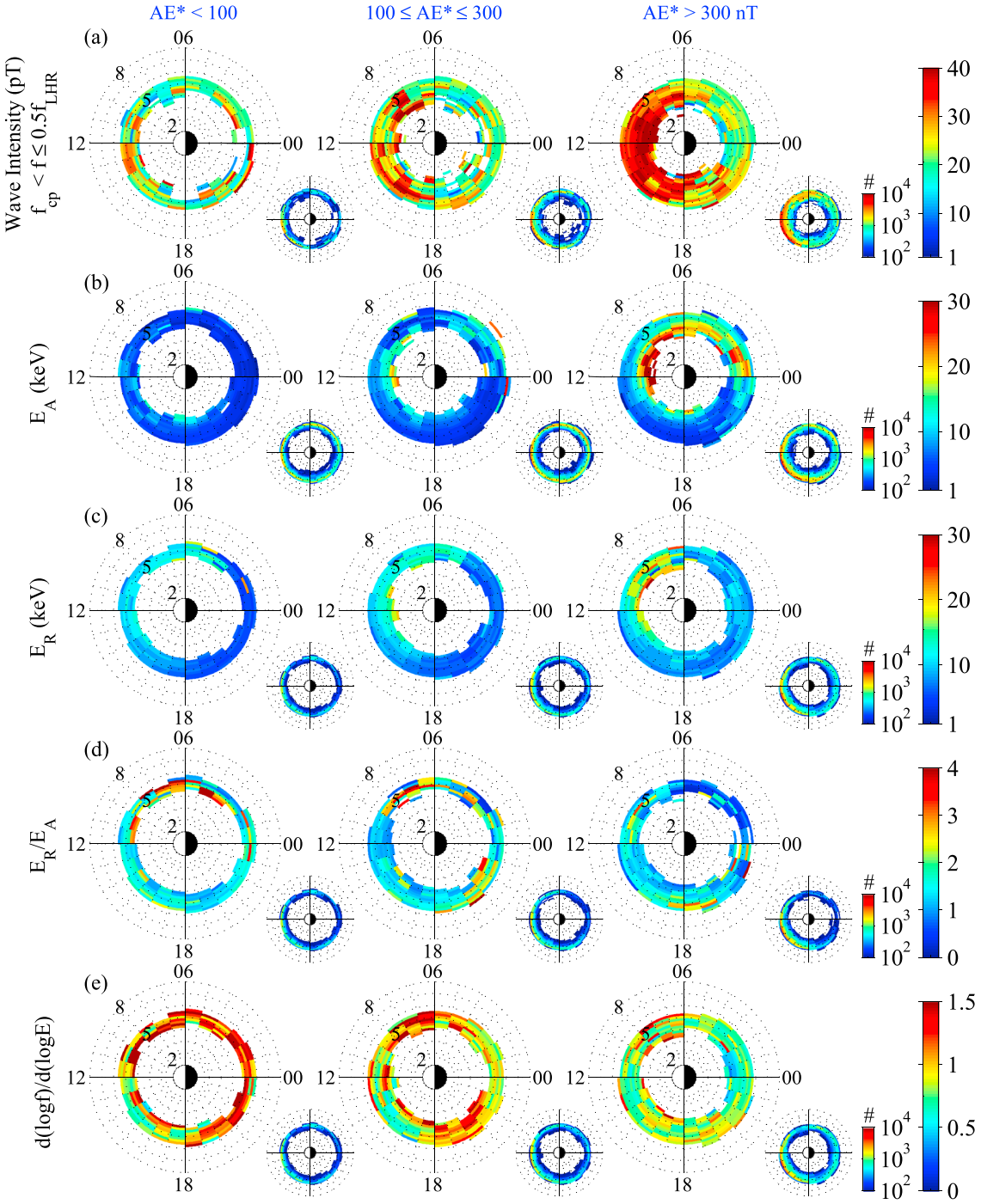

Figure 9. The global distribution of (a) magnetosonic wave intensity in low-frequency band ($f_{cp} < f \leq 0.5\ f_{LHR}$) outside the plasmapause and the corresponding quantities, (b) E_A, (c) E_R, (d) E_R/E_A, and (e) the logarithmic slope d(log$f$)/d(log$E$) between E_R and E_{dip}. The number of samples in each panel are shown in the small panels.

5. Discussion

The analysis shown in Figures 5–7 shows that the excitation of low-frequency magnetosonic waves in the prenoon sector outside the plasmapause might not be related to a proton ring distribution. To understand in more detail how the prenoon waves outside the plasmapause are excited (or enhanced), we present in Figure 9 the global distribution of (a) magnetosonic waves in a low-frequency band outside the

plasmapause for three levels of *AE**, together with the quantities (b) E_A, (c) E_R, (d) E_R/E_A, and (e) the logarithmic slope d(log*f*)/d(log*E*) between E_R and E_{dip}. As already well known, positive $df_\perp/dv_\perp$ at velocities just below V_R is associated with the magnetosonic wave growth (see equation (2) in Horne et al., 2000). Thus, for the present study, $df_\perp/dE_\perp$ with respect to $E_\perp$ between E_R and E_{dip} is simply adopted as the representative slope required for the excitation of magnetosonic waves, instead of estimating all the slopes for all available energy channels. It is estimated using the numerical approximation of $\frac{\log\left(f_{\perp,R}/f_{\perp,dip}\right)}{\log\left(E_R/E_{dip}\right)}$ following Thomsen et al. (2011).

As *AE** increases, the magnetosonic wave amplitude in the low-frequency band is considerably enhanced in the prenoon sector, together with an increase in both E_A and E_R. However, the E_A noticeably increase (mostly due to decrease in plasma density) while the E_R gradually increase, resulting in a generally gradual decrease in E_R/E_A in the prenoon sector with increasing *AE**, which is opposite to the tendency of variation in magnetosonic wave amplitude. There is also a significant decrease in the positive slopes with *AE** activity over a wide range of MLT, but they tend to peak around the prenoon sector during active times, which is qualitatively similar to the previous finding of Thomsen et al. (2011) using ion distributions observed at geosynchronous orbit. For the present study, we only focused on relative comparison of the positive slope among regions and *AE** values rather than on pointing out its value, since it is difficult to set a threshold for a significant positive slope that drives magnetosonic instability unless we calculate the growth rate, which is beyond the scope of this study (though Thomsen et al., 2011 set it as +0.3 for the slope at any given energy). The results suggest that the ratio $E_R/E_A \leq$ ~4 (corresponding to V_R/V_A ~ 2, which is suggested by Horne et al., 2000 and Chen et al., 2010) with relative high positive slopes around the prenoon sector against other regions at high *AE** activity favors the local excitation of magnetosonic waves at low frequencies outside the plasmapause, although the occurrence rate of proton rings in that region is relatively low compared to other regions, as shown in Figure 5b.

However, we cannot ignore the possibility, due to favorable conditions of high occurrence of proton rings and $E_R/E_A \leq$ ~1 for excitation of magnetosonic waves in the postnoon sector (12–18 MLT), that waves in the prenoon sector may have propagated azimuthally from the postnoon sector where they were excited. In addition, Kim and Shprits (2017) suggested that magnetosonic waves inside the plasmapause are enhanced around the prenoon sector during active times, and we thus speculate that they may have radially propagated out of the plasmasphere through the plasmapause in the prenoon sector (e.g., Xiao et al., 2012). More theoretical analysis and modeling should be done in the future to validate these observational results. In addition, the plasma beta (β) parameter, which is defined as a ratio of the plasma pressure to the magnetic pressure, is also known as one of the necessary conditions to diagnose wave instability. Gary et al. (2010) using linear kinetic dispersion theory showed that wave properties change significantly with β and suggested an appropriate value of β for maximum instability growth rate of ion Bernstein mode waves. Therefore, considering more kinetic properties of the plasma during the observation of fast magnetosonic waves may help to find the source of the waves, and whether they generated locally or not.

6. Conclusions

We have investigated the relationship between proton rings and magnetosonic waves in two frequency bands, $f_{cp} < f \leq 0.5\ f_{LHR}$ and $0.5\ f_{LHR} < f < f_{LHR}$ using particle and wave data from Van Allen Probe-A during the period from October 2012 to December 2015. The global distribution of particle data for protons at different energies showed that an unstable proton ring distribution is driven by energy-dependent drift: eastward gradient-curvature drift for >10 keV and westward $E \times B$ drift for a several keV. In addition, the clear statistical relationship between the proton rings and the magnetosonic waves suggests that proton rings are a potential source of the magnetosonic waves. We have also found that outside the plasmapause, the low E_R/E_A ratio ($\leq$ ~1) favors the excitation of magnetosonic waves in both low- and high-frequency bands in the postnoon sector (12–18 MLT), and waves in the low-frequency bands are observed in the prenoon sector (6–12 MLT), which is attributed to either that they may be locally excited in the region of a relatively high E_R/E_A ratio ($\leq$ ~4) or they may have originated from the postnoon sector via azimuthal propagation after being excited under the condition of proton rings with low E_R/E_A ($\leq$ ~1). Meanwhile, inside the plasmapause, a relatively higher E_R/E_A ratio (but less than ~9) than outside allow for excitation of the low-frequency band ($f_{cp} < f \leq 0.5 f_{LHR}$) of magnetosonic waves around the postnoon sector, while $E_R/E_A >$ ~9 inhibits excitation of

the magnetosonic waves. Our statistical results using Van Allen Probe-A are consistent with the previous theoretical and observational studies.

Acknowledgments
This research was supported by the Daegu University Research grant 20160376. We thank the GSFC/SPDF OMNIWeb for the provision of *AE* index used in this report. The Van Allen Probe data are available from http://emfisis.physics.uiowa.edu/Flight and from https://rbsp-ect.lanl.gov/data_pub/rbspa. We graciously thank the Van Allen Probes team, especially the EMFISIS and ECT teams. The electron number density derived by Neural-network-based Upper hybrid Resonance Determination algorithm for the Van Allen Probes is available from ftp://rbm.epss.ucla.edu/ftpdisk1/NURD.

References

Balikhin, M. A., Shprits, Y. Y., Walker, S. N., Chen, L., Cornilleau-Wehrlin, N., Dandouras, I., … Weiss, B. (2015). Observations of discrete harmonics emerging from equatorial noise. *Nature Physics*, *6*, 7703. https://doi.org/10.1038/ncomms8703

Boardsen, S. A., Gallagher, D. L., Gurnett, D. A., Peterson, W. K., & Green, J. L. (1992). Funnel-shaped, low-frequency equatorial waves. *Journal of Geophysical Research*, *97*(A10), 14967–14,976. https://doi.org/10.1029/92JA00827

Chen, L., Thorne, R. M., Jordanova, V. K., & Horne, R. B. (2010). Global simulation of magnetosonic wave instability in the storm time magnetosphere. *Journal of Geophysical Research*, *115*, A11222. https://doi.org/10.1029/2010JA015707

Chen, L., Thorne, R. M., Jordanova, V. K., Thomsen, M. F., & Horne, R. B. (2011). Magnetosonic wave instability analysis for proton ring distributions observed by the LANL magnetospheric plasma analyzer. *Journal of Geophysical Research*, *116*, A03223. https://doi.org/10.1029/2010JA016068

Convery, P. D., & Gary, S. P. (1997). Electromagnetic proton cyclotron ring instability: Threshold and saturation. *Journal of Geophysical Research*, *102*(A2), 2351–2358. https://doi.org/10.1029/96JA02951

Curtis, S., & Wu, C. (1979). Gyroharmonic emissions induced by energetic ions in the equatorial plasmasphere. *Journal of Geophysical Research*, *84*(A6), 2597–2607. https://doi.org/10.1029/JA084iA06p02597

Fok, M.-C., Moore, T. E., Kozyra, J. U., Ho, G. C., & Hamilton, D. C. (1995). Three-dimensional ring current decay model. *Journal of Geophysical Research*, *100*(A6), 9619–9632. https://doi.org/10.1029/94JA03029

Fok, M.-C., Moore, T. E., & Greenspan, M. E. (1996). Ring current development during storm main phase. *Journal of Geophysical Research*, *101*(A7), 15,311–15,322. https://doi.org/10.1029/96JA01274

Funsten, H. O., Skoug, R. M., Guthrie, A. A., MacDonald, E. A., Baldonado, J. R., Harper, R. W., … Chen, J. (2013). Helium, Oxygen, Proton, and Electron (HOPE) mass spectrometer for the Radiation Belt Storm Probes mission. *Space Science Reviews*, *179*(1-4), 423–484. https://doi.org/10.1007/s11214-013-9968-7

Gary, S. P., Liu, K., Winske, D., & Denton, R. E. (2010). Ion Bernstein instability in the terrestrial magnetosphere: Linear dispersion theory. *Journal of Geophysical Research*, *115*, A12209. https://doi.org/10.1029/2010JA015965

Horne, R. B., Wheeler, G. V., & Alleyne, H. S. C. K. (2000). Proton and electron heating by radially propagating fast magnetosonic waves. *Journal of Geophysical Research*, *105*(A12), 27,597–27,610. https://doi.org/10.1029/2000JA000018

Horne, R. B., Thorne, R. M., Glauert, S. A., Meredith, N. P., Pokhotelov, D., & Santolík, O. (2007). Electron acceleration in the Van Allen radiation belts by fast magnetosonic waves. *Geophysical Research Letters*, *34*, L17107. https://doi.org/10.1029/2007GL030267

Hrbáčková, Z., Santolík, O., Němec, F., Macúšová, E., & Cornilleau-Wehrlin, N. (2015). Systematic analysis of occurrence of equatorial noise emissions using 10 years of data from the Cluster mission. *Journal of Geophysical Research: Space Physics*, *120*, 1007–1021. https://doi.org/10.1002/2014JA020268

Jordanova, V. K., Kistler, L. M., Kozyra, J. U., Khazanov, G. V., & Nagy, A. F. (1996). Collisional losses of ring current ions. *Journal of Geophysical Research*, *101*(A1), 111–126. https://doi.org/10.1029/95JA02000

Jordanova, V. K., Farrugia, C. J., Quinn, J. M., Torbert, R. B., Borovsky, J. E., Sheldon, R. B., & Peterson, W. K. (1999). Simulation of off-equatorial ring current ion spectra measured by polar for a moderate storm at solar minimum. *Journal of Geophysical Research*, *104*(A1), 429–436. https://doi.org/10.1029/98JA02658

Kasahara, Y., Kenmochi, H., & Kimura, I. (1994). Propagation characteristics of the ELF emissions observed by the satellite Akebono in the magnetic equatorial region. *Radio Science*, *29*(4), 751–767. https://doi.org/10.1029/94RS00445

Kim, K.-C., & Chen, L. (2016). Modeling the storm time behavior of the magnetosonic waves using solar wind parameters. *Journal of Geophysical Research: Space Physics*, *121*, 446–458. https://doi.org/10.1002/2015JA021716

Kim, K.-C., & Shprits, Y. (2017). Dependence of the amplitude of magnetosonic waves on the solar wind and *AE* index using Van Allen Probes. *Journal of Geophysical Research: Space Physics*, *122*, 6022–6034. https://doi.org/10.1002/2017JA024094

Kletzing, C. A., Kurth, W. S., Acuna, M., MacDowall, R. J., Torbert, R. B., Averkamp, T., … Tyler, J. (2013). The Electric and Magnetic Field Instrument Suite and Integrated Science (EMFISIS) on RBSP. *Space Science Reviews*, *179*(1-4), 127–181. https://doi.org/10.1007/s11214-013-9993-6

Korth, H., Thomsen, M. F., Borovsky, J. E., & McComas, D. J. (1999). Plasma sheet access to geosynchronous orbit. *Journal of Geophysical Research*, *104*(A11), 25,047–25,061. https://doi.org/10.1029/1999JA900292

Laakso, H., Junginger, H., Roux, A., Schmidt, R., & deVilledary, C. (1990). Magnetosonic waves above fc (H+) at geostationary orbit: GEOS 2 results. *Journal of Geophysical Research*, *95*(A7), 10,609–10,621. https://doi.org/10.1029/JA095iA07p10609

Li, W., Ma, Q., Thorne, R. M., Bortnik, J., Kletzing, C. A., Kurth, W. S., … Nishimura, Y. (2015). Statistical properties of plasmaspheric hiss derived from Van Allen Probes data and their effects on radiation belt electron dynamics. *Journal of Geophysical Research: Space Physics*, *120*, 3393–3405. https://doi.org/10.1002/2015JA021048

Li, J., Bortnik, J., Li, W., Ma, Q., Thorne, R. M., Kletzing, C. A., … Russell, C. T. (2017). "Zipper-like" periodic magnetosonic waves: Van Allen Probes, THEMIS, and magnetospheric multiscale observations. *Journal of Geophysical Research: Space Physics*, *122*, 1600–1610. https://doi.org/10.1002/2016JA023536

Liu, K., Gary, S. P., & Winske, D. (2011). Excitation of magnetosonic waves in the terrestrial magnetosphere: Particle-in-cell simulations. *Journal of Geophysical Research*, *116*, A07212. https://doi.org/10.1029/2010JA016372

Lyons, L. R., & Williams, D. J. (1984). *Quantitative aspects of magnetospheric physics* (pp. 79–86). New York: Springer. https://doi.org/10.1007/978-94-017-2819-5

Ma, Q., Li, W., Thorne, R. M., & Angelopoulos, V. (2013). Global distribution of equatorial magnetosonic waves observed by THEMIS. *Geophysical Research Letters*, *40*, 1895–1901. https://doi.org/10.1002/grl.50434

Ma, Q., Li, W., Chen, L., Thorne, R. M., & Angelopoulos, V. (2014). Magnetosonic wave excitation by ion ring distributions in the Earth's inner magnetosphere. *Journal of Geophysical Research: Space Physics*, *119*, 844–852. https://doi.org/10.1002/2013JA019591

Ma, Q., Li, W., Thorne, R. M., Bortnik, J., Kletzing, C. A., Kurth, W. S., & Hospodarsky, G. B. (2016). Electron scattering by magnetosonic waves in the inner magnetosphere. *Journal of Geophysical Research: Space Physics*, *121*, 274–285. https://doi.org/10.1002/2015JA021992

Mauk, B. H., Fox, N. J., Kanekal, S. G., Kessel, R. L., Sibeck, D. G., & Ukhorskiy, A. (2012). Science objectives and rationale for the Radiation Belt Storm Probes mission. *Space Science Reviews*, 1–15. https://doi.org/10.1007/s11214-012-9908-y

McIlwain, C. E. (1961). Coordinates for mapping the distribution of magnetically trapped particles. *Journal of Geophysical Research*, *66*(11), 3681–3691. https://doi.org/10.1029/JZ066i011p03681

Meredith, N. P., Horne, R. B., Thorne, R. M., Summers, D., & Anderson, R. R. (2004). Substorm dependence of plasmaspheric hiss. *Journal of Geophysical Research*, *109*(A6), A06209. https://doi.org/10.1029/2004JA010387

Meredith, N. P., Horne, R. B., & Anderson, R. R. (2008). Survey of magnetosonic waves and proton ring distributions in the Earth's inner magnetosphere. *Journal of Geophysical Research*, *113*(A6), A06213. https://doi.org/10.1029/2007JA012975

Min, K., Liu, K., & Gary, S. P. (2017). Proton velocity ring-driven instabilities and their dependence on the ring speed: Linear theory. *Journal of Geophysical Research: Space Physics*, *122*, 7891–7906. https://doi.org/10.1002/2017JA023944

Moya, P. S., Pinto, V. A., Viñas, A. F., Sibeck, D. G., Kurth, W. S., Hospodarsky, G. B., & Wygant, J. R. (2015). Weak kinetic Alfvén waves turbulence during the 14 November 2012 geomagnetic storm: Van Allen Probes observations. *Journal of Geophysical Research: Space Physics*, *120*(7), 5504–5523. https://doi.org/10.1002/2014JA020281

Němec, F., Santolík, O., Pickett, J. S., Hrbáčková, Z., & Cornilleau-Wehrlin, N. (2013). Azimuthal directions of equatorial noise propagation determined using 10 years of data from the Cluster spacecraft. *Journal of Geophysical Research: Space Physics*, *118*, 7160–7169. https://doi.org/10.1002/2013JA019373

Perraut, S., Roux, A., Robert, P., Gendrin, R., Sauvaud, J.-A., Bosqued, J.-M., … Korth, A. (1982). A systematic study of ULF waves above FH+ from GEOS 1 and 2 measurements and their relationships with proton ring distributions. *Journal of Geophysical Research*, *87*(A8), 6219–6236. https://doi.org/10.1029/JA087iA08p06219

Roederer, J. G. (1970). *Dynamics of geomagnetically trapped radiation*, (pp. 76–79). New York: Springer-Verlag. https://doi.org/10.1007/978-3-642-49300-3

Russell, C. T., Holzer, R. E., & Smith, E. J. (1970). OGO 3 observations of ELF noise in the magnetosphere: 2. The nature of the equatorial noise. *Journal of Geophysical Research*, *75*(4), 755–768. https://doi.org/10.1029/JA075i004p00755

Salem, C. S., Howes, G. G., Sundkvist, D., Bale, S. D., Chaston, C. C., Chen, C. H. K., & Mozer, F. S. (2012). Identification of kinetic Alfvén wave turbulence in the solar wind. *The Astrophysical Journal*, *745*(1), L9. https://doi.org/10.1088/2041-8205/745/1/L9

Santolík, O., Pickett, J. S., Gurnett, D. A., Maksimovic, M., & Cornilleau-Wehrlin, N. (2002). Spatiotemporal variability and propagation of equatorial noise observed by Cluster. *Journal of Geophysical Research*, *107*(A12), 1495. https://doi.org/10.1029/2001JA009159

Santolík, O., Parrot, M., & Lefeuvre, F. (2003). Singular value decomposition methods for wave propagation analysis. *Radio Science*, *38*(1), 1010. https://doi.org/10.1029/2000RS002523

Shprits, Y. Y. (2016). Estimation of bounce resonant scattering by fast magnetosonic waves. *Geophysical Research Letters*, *43*(3), 998–1006. https://doi.org/10.1002/2015GL066796

Shprits, Y. Y., Runov, A., & Ni, B. (2013). Gyro-resonant scattering of radiation belt electrons during the solar minimum by fast magnetosonic waves. *Journal of Geophysical Research: Space Physics*, *118*, 648–652. https://doi.org/10.1002/jgra.50108

Thomsen, M. F., Denton, M. H., Jordanova, V. K., Chen, L., & Thorne, R. M. (2011). Free energy to drive equatorial magnetosonic wave instability at geosynchronous orbit. *Journal of Geophysical Research*, *116*(A8), A08220. https://doi.org/10.1029/2011JA016644

Tsyganenko, N. A., & Sitnov, M. I. (2005). Modeling the dynamics of the inner magnetosphere during strong geomagnetic storms. *Journal of Geophysical Research*, *110*(A3), A03208. https://doi.org/10.1029/2004JA010798

Umeda, T., Ashour-Abdalla, M., Schriver, D., Richard, R. L., & Coroniti, F. V. (2007). Particle-in-cell simulation of Maxwellian ring velocity distribution. *Journal of Geophysical Research*, *112*(A4), A04212. https://doi.org/10.1029/2006JA012124

Umeda, T., Matsukiyo, S., Amano, T., & Miyoshi, Y. (2012). A numerical electromagnetic linear dispersion relation for Maxwellian ring-beam velocity distributions. *Physics of Plasmas*, *19*(7), 072107. https://doi.org/10.1063/1.4736848

Xiao, F., Zhou, Q., He, Z., & Tang, L. (2012). Three-dimensional ray tracing of fast magnetosonic waves. *Journal of Geophysical Research*, *117*(A6), A06208. https://doi.org/10.1029/2012JA017589

Zhelavskaya, I. S., Spasojevic, M., Shprits, Y. Y., & Kurth, W. S. (2016). Automated determination of electron density from electric field measurements on the Van Allen Probes spacecraft. *Journal of Geophysical Research: Space Physics*, *121*, 4611–4625. https://doi.org/10.1002/2015JA022132